Hydrodynamic investigation on the submerged tunnel suspended from a fixed platform using SPH method

Can Yang [a,b], Zhibin Hao [a,b], Ming He [c,*], Hailong Chen [a,b], Lars Johanning [a,b,d,*]
[a] Yantai Research Institute of Harbin Engineering University, Yantai 264000, China
[b] College of Shipbuilding Engineering, Harbin Engineering University, Harbin 150001, China
[c] State Key Laboratory of Hydraulic Engineering Simulation and Safety, Tianjin University, Tianjin 300072, China
[d] College of Engineering, Mathematics and Physical Sciences, University of Exeter, Penryn Campus, Penryn, Cornwall, TR10 9FE, UK

Abstract:

In this paper, the coupled dynamic motion characteristics of a tunnel element suspended from a platform have been studied at a 1:50 scaled model by using the weakly compressible Smoothed Particle Hydrodynamic (WCSPH) method. The corresponding numerical model was validated with the experimental published data of the motion characteristics of the tunnel suspended from a fixed platform, and the case of a floating structure with its mooring lines. Multiple linear wave conditions and different sinking depths of the submerged were involved in the numerical model for tunnel dynamic response and cable behavior investigation. Effects of the mooring system, the wave parameters, the tunnel sinking depth and its mooring configurations were studied. The numerical results were arranged to inform about the dynamic characteristics and mooring behavior for different case studies. The results indicate that the tunnel motions decrease with the increment of the tunnel sinking depth and decrease with the decreasing mooring angle. The natural periods of the tunnel-platform system play key roles in the wave condition impacts on the tunnel motions. It was found that the additional mooring system anchoring the tunnel to seabed played a specific role in reducing the tunnel motions in roll and sway, the motion amplitude of the tunnel in heave is mainly controlled by the suspension cables, particularly when subjected to lower sinking depth and longer period waves.

Keywords： Submerged tunnel; Platform; Motion response; Mooring system; SPH method

1. Introduction

With the growing economic development, the demands for the maritime transportation are constantly increasing. Compared with the cross-sea bridges, the main advantage of the submarine tunnel is that vessel navigation will not be hindered. Meanwhile, the requirements of the highly efficient maritime transportation can be achieved. Nowadays, the submerged tunnel has been widely applied due to its multiple advantages compared with the shield tunnel (Glerum, 1955; Janssen, 2006), such as prefabricated tunnel components onshore, a better quality of construction, lower construction cost, safety construction method, etc. (Fu, 2004; Ingerslev et al., 2012).

Due to the comparatively higher requirements of the design of the submerged tunnel, the severe weather conditions will remarkably affect the stability and safety of the tunnel during its lowering. Hence, the influence of the sea environment on the tunnel lowering has become a critical factor for design issue. Aono et al. (2003) conducted the model test and numerical analysis on the stability of the Naha Submerged Tunnel under wave impact with a significant wave height of 5.3 m. A rapid emplacement method is proposed to maintain the stability of the tunnel, which has been successfully applied to the installation work of submerged tunnel. Based on the physical tests and the numerical simulations, the stability of the submerged tunnel of the Busan–Geoje Fixed Link has been subjected to detailed studies by Kasper et al. (2008), experiencing the significant wave height up to 9.2 m. Nagel et al. (2011) investigated the effects of the swell waves on the tunnel element motions, and different buoyancy weight of the tunnel has been numerically and experimental tested for study the impacts on the tunnel dynamic response.

Meanwhile, the coupled dynamic behavior of the tunnel is more vulnerable to being frequently attacked by waves during its sinking process, which is sensitive to affect the positioning accuracy of the submerged tunnel. Therefore, it is exigent to investigate the hydrodynamic coupled characteristics of the tunnel and its lowering system subjected to waves, employing series of the model tests and numerical modellings. Chen et al. (2009a) carried out the experiment to investigate the motion response of the submerged tunnel element and the wave loads, in the physical model the mooring system is not considered. Chen et al. (2012) and Peng et al. (2012) experimentally and numerically investigated the dynamics of the tunnel-pontoon systems during an interruption in the sinking procedure, based on the Hong Kong-Zhu Hai-Macao Bridge project. Huang et al. (2019) experimentally analyzed the coupled motion characteristics of the tunnel and the immersion rig with its hoisting cable under different wave conditions. The results indicate that the coupling between the tunnel and rig was more vulnerable with longer period waves.

The Smoothed Particle Hydrodynamics (SPH) method has recently attracted wide attention since it was introduced into the hydrodynamic field by Monaghan (1994). It is well suited for handling fluid-structure interaction problems due to its complete mesh-free ability. Bouscasse et al. (2013) presented a weakly compressible SPH (WCSPH) solver for applications involving the nonlinear wave-structure interaction, based on a complete algorithm of computing the fully coupled viscous Fluid–Solid interactions. Ren et al. (2015) investigated the nonlinear interactions between the waves and the floating body, using the WCSPH method with an improved algorithm based on the dynamic boundary particles, which is proposed to deal with the moving boundary of the floating body and has been verified with the experiments. Bayareh et al. (2019) investigated the two-dimensional channel flow in the presence of a square solid object and lid-driven square cavity flow for both Newtonian and non-Newtonian fluids by using explicit incompressible SPH algorithm, it indicates that this method has a high ability to predict the behavior of non-Newtonian power law fluids. As evidenced by the above analysis, it is appropriate to apply SPH method to investigate the coupled interactions between the submerged tunnel and the complicated support system for lowering process. There is currently a lack of specific study on the lowering characteristics of the tunnel suspended from a fixed platform, for example, combined suspension cable and mooring behavior under resonant wave conditions and optimization of the cable and mooring configuration etc., solving the problem of the submerged tunnel is firstly investigated by using SPH method as well.

The present study aims to fill two major research gaps. The influence of the suspension cables as well as the mooring system on the dynamic response of the submerged tunnel element is firstly investigated under different immersion depths during tunnel immersion. Multiple wave condition effects and mooring configurations were applied. Hence, a numerical model of the submerged tunnel element suspended from a fixed platform subjected to waves was developed by using SPH method, to investigate the tunnel hydrodynamics and the coupled tension behavior of combined lowering support system. The paper is organized as follows. After the introduction, Section 2 introduced the methodology including the governing equations of WCSPH model and the coupled equations for solving the motion response of the submerged tunnel element. Then, the validations of the numerical modelling were carried out in Section 3, including the validation of the numerical wave flume, the mooring tensions of the floating structure and the motion response of the hoisting tunnel element, respectively. In Section 4, the validated numerical model is applied to investigate the effects of various wave climate, sinking depth of the tunnel and different mooring configurations on the dynamic behavior of both the tunnel motions and the combined hoisting-mooring system. The main conclusions and the perspectives in the future research are drawn in Section 5.

2. Methodology

Due to the advantage of meshfree particle resolution on solving the fluid-solid coupling problem, Smoothed Particle Hydrodynamics (SPH) method is used in this paper to simulate the dynamic response of the submerged tunnel element suspended from a platform. The motion response of the tunnel, the suspension cable tension and the mooring loads of the complicated couple system are calculated by using the proposed numerical model. The details of the governing equations, the motion equations, the fluid and cable force and the summary of the numerical set-up are presented in this section.

2.1 Governing equations of SPH

Kernel approximation and particle approximation are basically involved in obtaining the SPH formulation (Liu et al., 2010). Kernel approximation function and its derivative are represented in Eq.(1) and Eq.(2) respectively. Then, a finite number of the particles set in the computational domain, Eq.(3) and Eq.(4) represent the particle approximation and its derivative, respectively.

$$\langle f(\boldsymbol{x_0})\rangle = \int_\Omega f(\boldsymbol{x}) W(\boldsymbol{x_0}-\boldsymbol{x},h)\,d\boldsymbol{x} \tag{1}$$

$$\langle \nabla\cdot f(\boldsymbol{x_0})\rangle = -\int_\Omega f(\boldsymbol{x})\cdot\nabla W(\boldsymbol{x_0}-\boldsymbol{x},h)\,d\boldsymbol{x} \tag{2}$$

$$\langle f(\boldsymbol{x}_i)\rangle = \sum_{j=1}^{N}\frac{m_j}{\rho_j} f(\boldsymbol{x}_j) W_{ij} \tag{3}$$

$$\langle \nabla\cdot f(\boldsymbol{x}_i)\rangle = \sum_{j=1}^{N}\frac{m_j}{\rho_j} f(\boldsymbol{x}_j) \nabla_{\boldsymbol{i}} W_{ij} \tag{4}$$

In the above equations (3-4), subscripts *i* and *j* donate the target particle and the neighboring particle within the support of *i*. *N* is the total number of the neighboring particles, *h* represents the smoothing length. *m* and *ρ* represent the particle mass and density, respectively. ***x*** is the position vector, W_{ij} is the kernel function that replaces the Dirac delta function. In this paper, a quintic kernel suggested by Wendland (1995) is used:

$$W_{ij} = \frac{7}{4\pi h^2}\left(1-\frac{q}{2}\right)^4 (2q+1) \qquad 0\le q\le 2 \tag{5}$$

The flow fluid is governed by the Navier-Stokes equations (Eq.(6) and Eq.(7)), substituting the SPH particle approximations and its derivative (Eq.(3) and Eq.(4)) to the N-S equations, then the equations can be rewritten as Eq.(8) and Eq.(9).

$$\frac{D\rho}{Dt} = -\rho\nabla\cdot\boldsymbol{u} \tag{6}$$

$$\frac{D\boldsymbol{u}}{Dt} = -\frac{1}{\rho}\nabla p + \boldsymbol{g} + \boldsymbol{\Gamma} \tag{7}$$

$$\frac{d\rho_i}{dt} = \rho_i\sum_{j=1}^{N}\frac{m_j}{\rho_j}\left(\boldsymbol{u}_i-\boldsymbol{u}_j\right)\cdot\nabla_i W_{ij} \tag{8}$$

$$\frac{d\boldsymbol{u}_i}{dt} = -\sum_{j=1}^{N} m_j\left(\frac{p_j}{\rho_i^2}+\frac{p_j}{\rho_j^2}+\Pi_{ij}\right)\nabla_i W_{ij} + \boldsymbol{g} \tag{9}$$

where *ρ* is the density of the fluid, ***u*** is the velocity vector, *p* is the pressure, and *g* stands for the gravitational acceleration.

Furthermore, **Γ** is the dissipation term, the artificial viscosity proposed by Monaghan (1985) is used to eliminate the unphysical oscillations. The viscosity of the real fluid is neglected and an artificial viscosity term Π_{ij} is added in the Eq.(10), to produce a shear and bulk viscosity (Monaghan, 1992). Π_{ij} is given by

$$\Pi_{ij} = \begin{cases} \dfrac{-\alpha_{\Pi}\bar{c}_{ij}\mu_{ij} + \beta_{\Pi}\mu_{ij}^{2}}{\bar{\rho}_{ij}}, & \boldsymbol{u}_{ij}\cdot\boldsymbol{r}_{ij} < 0 \\ 0, & \boldsymbol{u}_{ij}\cdot\boldsymbol{r}_{ij} > 0 \end{cases} \tag{10}$$

where $\boldsymbol{u}_{ij}$ and $\boldsymbol{r}_{ij}$ are the relative velocity vector and relative space vector, respectively. $\boldsymbol{u}_{ij} = \boldsymbol{u}_i$-$\boldsymbol{u}_j$ and $\boldsymbol{r}_{ij} = \boldsymbol{r}_i$-$\boldsymbol{r}_j$. In addition, $\bar{c}_{ij}$ and $\bar{\rho}_{ij}$ denote the average speed of sound and the average density, which are given by $\bar{c}_{ij} = (c_i + c_j) / 2$, $\rho_{ij} = (\rho_i + \rho_j) / 2$, and $\boldsymbol{\mu}_{ij} = h\boldsymbol{u}_{ij} \cdot \boldsymbol{r}_{ij} / (\boldsymbol{r}_{ij}^{2} + 0.01h^2)$.

The fluid is assumed as the weakly compressible flow, the pressure is determined by solving the status equation. In this modelling, the equation of state (Eq.(11)) proposed by Monaghan and Kos (1999) is used.

$$p = \frac{c_0^2\rho_0}{\gamma}\left[\left(\frac{\rho}{\rho_0}\right)^{\gamma} - 1\right] \tag{11}$$

where c_0 is the speed of sound at the reference density ($c_0^2 = 200gd$), which is derived from the numerical speed of sound in a fluid medium by using SPH method, initially proposed by Monaghan and Kos (1999). d is the water depth, ρ_0 denotes the reference density, the value of ρ_0 is 1000 kg/m^3, and $\gamma = 7$.

The particles are set as the initial density of 10^3 kg/m. In gravity flows, it needs to correct the hydrostatic pressure for adjustment after the pressure obtained from the equation of state. For example, when the gravity acts in the negative z direction, the density is given by

$$\rho = \rho_0\left[1 + \frac{\rho_0 g\left(d - z\right)}{B}\right]^{1/\gamma} \tag{12}$$

where $B = c_0^2\rho_0/\gamma$, z is the vertical coordinate of the particle, and $z = 0$ is located at the bottom of the flume.

In order to smooth the high frequency fluctuations of the particle in the density and pressure field, a Shepard filter [33] is used to renormalize the density field in every 20 time-steps:

$$\rho_i = \frac{\sum_j m_j W_{ij}}{\sum_j \frac{m_j}{\rho_j} W_{ij}} \tag{13}$$

To reduce the randomness of the particles, the XSPH proposed by Monaghan (1989) is used to calculate the position of the particles:

$$\frac{d\boldsymbol{r}_i}{dt} = \boldsymbol{u}_i + \varepsilon\sum_{j=1}^{N}\frac{m_j}{\rho_{ij}}\left(\boldsymbol{u}_i - \boldsymbol{u}_j\right)W_{ij} \tag{14}$$

where ε is a constant value between 0 and 1, and ε is taken as 0.3 in this model.

In this paper, based on the Dynamic Boundary Conditions (DBC) proposed by Dalrymple and Knio (2001) and later explicated by Crespo et al. (2007), the Dynamic Boundary Particles (DBPs) are implemented with specific treatment by Ren et al. (2015) is used:

$$\rho_i^{'} = \chi\rho_i + \left(1 - \chi\right)\frac{1}{N}\sum_{j=1}^{N}\left(\rho_j + \frac{\partial\rho_j}{\partial r}\left(r_j - r_i\right)\right) \tag{15}$$

where ρ_i and ρ_i' are the density of DBPs and its modification, respectively. χ is a weighted coefficient between 0 and 0.5, which is chosen as 0.2. j is the fluid particles in the kernel support, and N is the total number of the particles. $\partial\rho_j/\partial$r (r_i-r_j) is a correction term.

According to the reference by Antuono et al. (2015), Δt_a and Δt_c are calculated based on the particle acceleration and the viscosity conditions, respectively. Meanwhile, the time step Δt is chosen as the minimum value (Δt=min (Δt_a, Δt_c)) as follows

$$\Delta t_a \le 0.25\min_i\sqrt{\frac{h}{\left\|\boldsymbol{a}_i\right\|}} \tag{16}$$

$$\Delta t_c \le CFL\min_i\left(\frac{h}{c0 + h\max_j\left|\pi_{ij}\right|}\right) \tag{17}$$

in which $||\boldsymbol{a}_i||$ is the particle acceleration, the value of *CFL* in the Predictor-Corrector scheme is normally chosen within the range [0.1, 0.3] (Green, 2016), and taken as 0.2 in the present work. π_{ij} (Antuono et al., 2012) is calculated by

$$\pi_{ij} = \frac{(\boldsymbol{u}_j - \boldsymbol{u}_i)\cdot(\boldsymbol{r}_j - \boldsymbol{r}_i)}{|\boldsymbol{r}_j - \boldsymbol{r}_i|^2} \tag{18}$$

2.2 Motion equations of submerged tunnel

The force analysis diagram of the submerged tunnel element with its lowering system in water wave is shown in Fig. 1. The tunnel element is suspended from a fixed platform, the upper of the tunnel is jointed and supported by the suspension cable lines. The tunnel element is tensioned with its mooring system and anchored to the seabed.

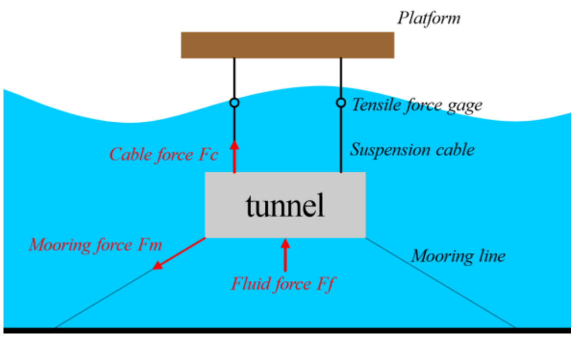

Fig. 1. Diagram of the force analysis for submerged tunnel element

The motion of the submerged tunnel element follows Newton's second law, and the centroid motion and rotation of the tunnel are given by

$$\begin{cases} M\dfrac{d\boldsymbol{v}}{dt} = (\boldsymbol{F}_c + \boldsymbol{F}_m + \boldsymbol{F}_f) + M\boldsymbol{g} \\ I\dfrac{d\boldsymbol{\varpi}}{dt} = (\boldsymbol{T}_c + \boldsymbol{T}_m + \boldsymbol{T}_f) \end{cases} \tag{19}$$

where *M* is the mass of the tunnel, *I* is the inertia moment of the tunnel, $\boldsymbol{v}$ and $\boldsymbol{\omega}$ are the centroid linear velocity and the centroid angular velocity, respectively. $\boldsymbol{F}_f$, $\boldsymbol{F}_m$ and $\boldsymbol{F}_c$ are the fluid loads, the mooring force and the cable tension acting on the submerged tunnel. $\boldsymbol{T}_c$, $\boldsymbol{T}_m$ and $\boldsymbol{T}_f$ are the corresponding moments of $\boldsymbol{F}_c$, $\boldsymbol{F}_m$ and $\boldsymbol{F}_f$.

A series of solid boundary particles are set on the boundary of the tunnel, the velocity of the boundary particle is given by

$$\frac{d\boldsymbol{r}_i}{dt} = \boldsymbol{u}_i = v + \boldsymbol{\varpi} \times (\boldsymbol{r}_i - \boldsymbol{r}_o) \tag{20}$$

where subscript *i* denotes the solid boundary particle; $\boldsymbol{r}_i$ and $\boldsymbol{r}_o$ are the position of the solid boundary particle and the mass center of the tunnel, respectively.

The fluid force $\boldsymbol{f}_i$ acting on the DBP from the neighboring fluid particles is calculated as following:

$$\boldsymbol{f}_i = m_i\frac{d\boldsymbol{u}_i}{dt} = m_i\left[-\sum_{j=1}^{N} m_j\left(\frac{p_j}{\rho_i^2} + \frac{p_j}{\rho_j^2} + \Pi_{ij}\right)\nabla_i W_{ij} + \boldsymbol{g}\right] \tag{21}$$

By summing up $\boldsymbol{f}_i$ on all DBPs, the global fluid force $\boldsymbol{F}_f$ and the moment $\boldsymbol{T}_f$ acting on a module can be calculated by

$$\boldsymbol{F}_f = \sum_i \boldsymbol{f}_i \tag{22}$$

$$\boldsymbol{T}_f = \sum_i \left(\boldsymbol{r}_i - \boldsymbol{r}_o\right) \times \boldsymbol{f}_i \tag{23}$$

In this paper, the tunnel element is assumed to be continuously lowered by the type of mooring system with a tensioning wheel. Thus, for different immersion depth of the tunnel, the mooring lines are set to be tensioning in the numerical model. Then, the mooring lines as well as the suspension cables are simulated as a tensible line with a lightweight spring, such cable lines can only bear tensile forces and according to Hooke's law the mooring force can be calculated as

$$\boldsymbol{F}_m = \begin{cases} k_m\left(l_m - l_{m0}\right), & l_m > l_{m0} \\ 0, & l_m < l_{m0} \end{cases} \tag{24}$$

$$\boldsymbol{T}_m = \left(\boldsymbol{r}_m - \boldsymbol{r}_o\right) \times \boldsymbol{F}_m \tag{25}$$

$$\boldsymbol{F}_c = \begin{cases} k_c\left(l_c - l_{c0}\right), & l_c > l_{c0} \\ 0, & l_c < l_{c0} \end{cases} \tag{26}$$

$$\boldsymbol{T}_c = \left(\boldsymbol{r}_c - \boldsymbol{r}_o\right) \times \boldsymbol{F}_c \tag{27}$$

For the above equations, the subscript symbol m and c represent the components of the mooring line and the cable line, respectively. For example, l_c is the suspension cable line length and l_m is the mooring line length. l_{c0} and l_{m0} represent the initial length of the suspension cable and mooring line, respectively. k_m is the mooring stiffness and k_c is the hoisting stiffness of the cable.

2.3 Numerical flume and model setup

To reduce the influence of the secondary reflection of the waves in the numerical flume testing area, the active-absorbing wave generation technique proposed by Hirakuchi et al.(1990) was applied. The motion of the wavemaker in the numerical flume is calculated by

$$V = \frac{\partial X_m}{\partial t} = \frac{\omega}{T_0}\left[2\eta_P - \eta_m + DX_m\right] \tag{28}$$

where X_m is the displacement of the wavemaker, $\omega=2\pi/T$ is represented as the angular frequency of the wave, η_p and η_m are the target and measured surface elevations at the wave paddle, respectively. T_0 is the transfer function of the evanescent mode

$$T_0 = \frac{4\sinh^2(kd)}{2kd + \sinh(2kd)} \tag{29}$$

where k is denoted as the wave number, and the parameter D is calculated by

$$D = \sum_{n=1}^{\infty} T_n = \frac{4\sinh^2(k_n d)}{2k_n d + \sinh(2k_n d)} \tag{30}$$

in which k_n is an imaginary wave number, which can be calculated by the dispersion relation as follows

$$\omega^2 = -k_n g \tanh k_n d \tag{31}$$

A sponge layer is arranged at the end of the flume to absorb the wave reflection, by adding a damping term to the fluid momentum equation to reduce the speed of the water particle movements. An artificial damping term $\mu(x)\cdot\boldsymbol{u}_i$ is added to the momentum equation (Eq.(9)), where $\mu(x)$ is calculated by

$$\mu(x) = \alpha\frac{\left|x - x_0\right|}{l_s} \qquad x_0 < x < x_0 + l_s \tag{32}$$

in which α is the sponge layer coefficient that is chosen in reference (Carmigniani et al., 2018); x_0 and l_s are the initial position and the length of the sponge layer, respectively.

Fig. 2 shows the numerical flume and the tunnel element model suspended from the platform located in the testing area in the central of the flume. A Froude model scale of 1:50 was chosen for numerical simulation is consistent with the experimental results that of the tunnel lowering from a floating twin-barge (Yang, 2017), to investigate the characteristics between different lowering methods. The numerical flume setup and the testing wave conditions are introduced in Table 1. The main properties of the tunnel-platform system are simulated according to the prototype values as summarized in Table 2, and the local coordinate origins of the tunnel element were on the centroid of the tunnel.

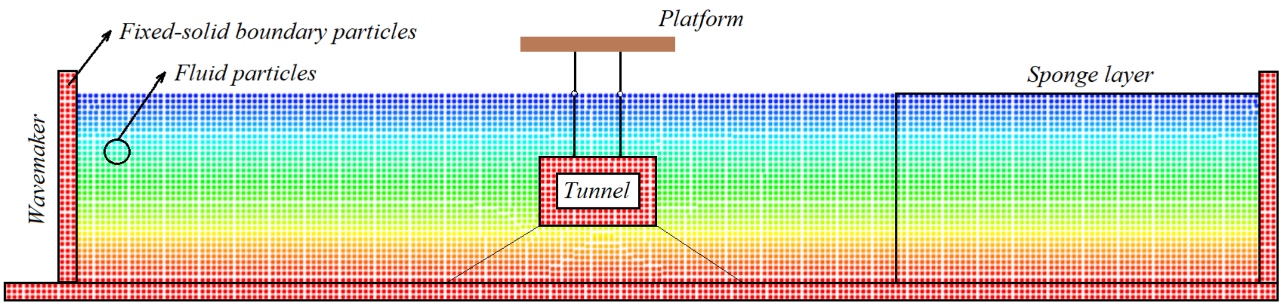

Fig. 2. Numerical wave flume based on SPH

Table 1

Properties of numerical wave flume and testing wave conditions.

Flume length (m)	Flume width (m)	Flume height (m)	Wavemaker position (m)	Water depth (m)	Sinking depth of tunnel (m)	Testing wave periods (s)	Testing wave height (m)
9.21	1.0	0.9	0.5	0.8	0.3-0.5	0.95-1.4	0.03-0.05

In the numerical model, the suspension cables and mooring lines are symmetrically arranged, they are located on the onshore side and offshore side of the tunnel element. The arrangement of the mooring system is parallel-shape in *x*-*y* plane, and the angle between the wave direction and the mooring lines is 45°, as is shown in Fig.2. The suspension cables are calculated as the springs with stiffness and the wire ropes with negligible weight which is represented at small-scale, the stiffness and weight properties which are Froude scaled from the full-scale hoisting cables, the simplified properties of the suspension cable and mooring system for the tunnel-platform in the numerical model are shown in Table 2. For simplification, it is assumed that the cable tension is equal at any position when it is in tension, while the cable force acting on the tunnel and platform is equal to zero when it is slack. Hence, the suspension cable and mooring system maybe commutatively support the tunnel in every time step during its immersion stage.

Table 2

Main model properties of tunnel-platform system.

Component	Parameter (unit)	Model scale	Prototype
Tunnel element	Length (m)	1	50
	Width (m)	0.3	15
	Height (m)	0.2	10
	Weight in water (N)	600.25	0.375×10^8
	Center of buoyancy (m) [a]	0.099	4.93
Cable-mooring system	Cable stiffness k_c (N/m)	1.4×10^3, 5.8×10^3	1.75×10^8, 7.25×10^8
	Cable length (m)	0.34, 0.44, 0.54	17, 22, 27
	Mooring stiffness k_m (N/m)	3.4×10^3, 7.4×10^3	4.25×10^8, 9.25×10^8

	Mooring length(m)	0.69, 0.52, 0.34	34.5, 26, 17
	mooring angle θ (°)	75, 60, 45, 30	75, 60, 45, 30

[a] COB measured from the bottom of the twin-barge/tunnel element.

3. Modelling validations

In this section, a series of the validation cases are carried out to validate the numerical model by comparing the computational and the experimental results. Modelling convergence is also tested to determine an optimal spatial resolution.

3.1 Numerical flume verification

Firstly, the wave generation performance of the numerical flume is given to compare the computed time histories of the wave elevations with different initial interparticle distance d_p to create the fluid and boundary particles in SPH. The generated wave height should be accurately calculated by the appropriate initial interparticle distance according to the study of Altomare et al. (2017). Hence, four spatial resolutions of H/d_p=0.5, 1.0, 3.0 and 6.0 are chosen to examine the numerical convergence of the SPH model for validation. For example, when the wave height is of H=0.03 m, the corresponding d_p are 0.06m, 0.03m,0.01m and 0.005m, allowing a total number of particles generated with these different resolutions of 1741, 5968, 48329 and 187004.

Fig. 3 provides a comparison between numerical and theoretical results of the generated wave elevation history at two measured wave gauges 1# and 2#, which were arranged at 0.5m and 1.0m in front of the tunnel element, respectively. Based on the active-absorbing wavemaker and sponge layer technique using WCSPH, numerical values are obtained for four different resolutions (d_p =0.06m, d_p =0.03m, d_p =0.01m and d_p =0.005m), good agreement can be seen with the theoretical value of the generated wave height (H=0.03 m). The computed results show that the computational results of the wave elevation with four different spatial resolutions are close to each other, and the difference between the finer computations is lower, compared with the difference between the coarser ones. Accordingly, considering the calculation accuracy and calculation efficiency, the most refined computation has been found throughout the comparisons (d_p =0.01m). Meanwhile, the convergence of the established numerical mode is validated.

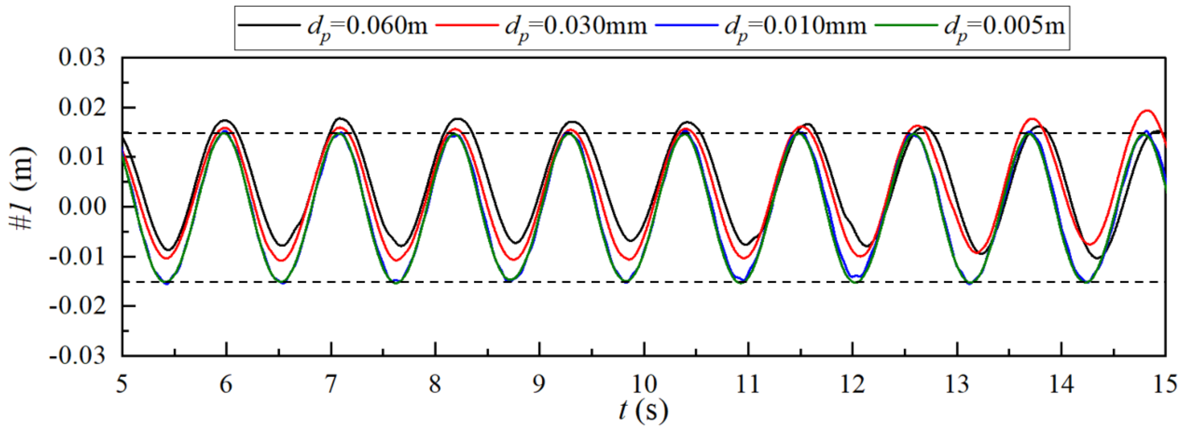

(a)

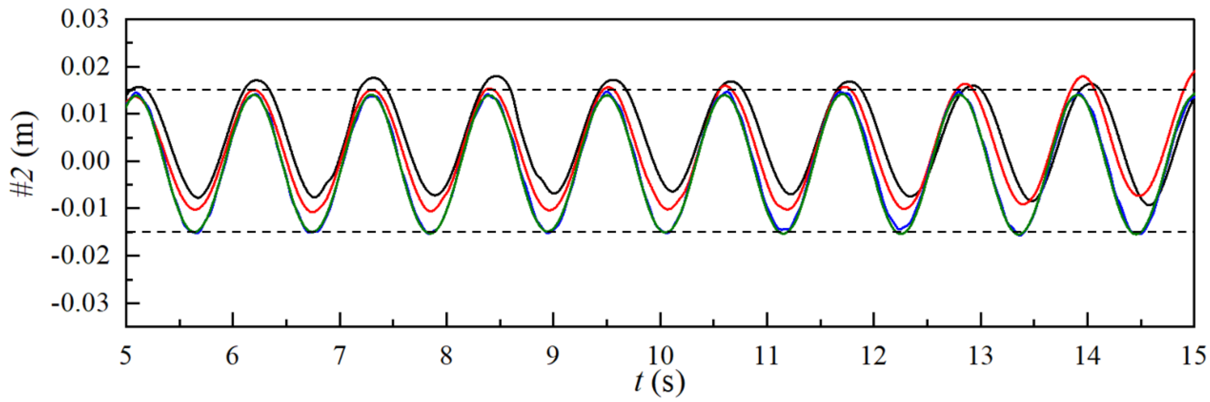

(b)

Fig. 3. Comparison of the computed time histories of the wave elevations at (a) 1# and (b) 2# wave gauges

3.2 Verification of floating body with mooring line

To verify the mooring characteristics of the floating body, a validation test is carried out to compare with Peng et al. (2013) that studied the interaction between a submerged floating body and its mooring lines by conducting the physical experiments. In this experiment, the wave tank was 30m in long, 0.7m in width and 0.9m in depth, a piston-type wavemaker and a rubble mound were used to generate waves and absorb waves, respectively. The moored submerged pontoon was 0.40 m long, 0.15 m high and 0.68 m wide. The mass and moment of the inertia for the pontoon are 28.6 kg and 0.435 kg·m^2, respectively. The anchor angle of the mooring system is of 60°. According to this, a corresponding SPH model is established, and the testing conditions are set as the same as the experiment, as is shown in Fig. 4. Regular wave with the wave height of 0.046m and wave period of 1.0 s is simulated in the numerical model. For simplification, the taut stainless chains in the physical tests were simulated as a light spring with the mooring stiffness of k_m =10^6 N/m in the modelling. A wave gauge set at the seaward side of the floating buoy was selected to record the measured wave surface in the numerical model, as is seen in Fig. 4.

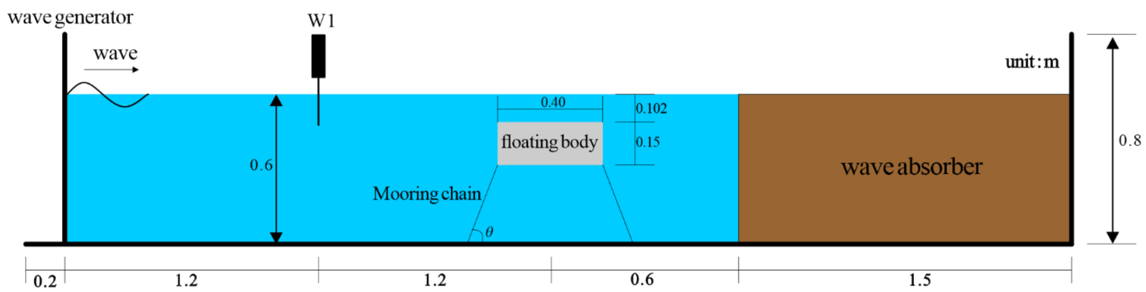

Fig. 4. Sketch of the moored pontoon model for validation of mooring characteristics

Fig.5 compares the wave surface elevations at the position of the wave gauge(#W1) which located at 1.2m from the wave generator, for numerical and experimental results. The simulated numerical wave surface is in good agreement with the published experimental data, and the numerical generated wave height matches well with the setting wave height property. Besides, the modeled motion responses of the pontoon buoy compared with the experimental results are provides in Fig. 6. Comparatively the modeled and experimental results of the pontoon's motions in sway, heave and roll directions agree very well, with the SPH model able to replicate the measured motion amplitude of the floating body with mooring system, albeit with a slightly difference of the dynamic response of the moored pontoon in heave, which may be caused by the simplification of the taut chain model in the simulation.

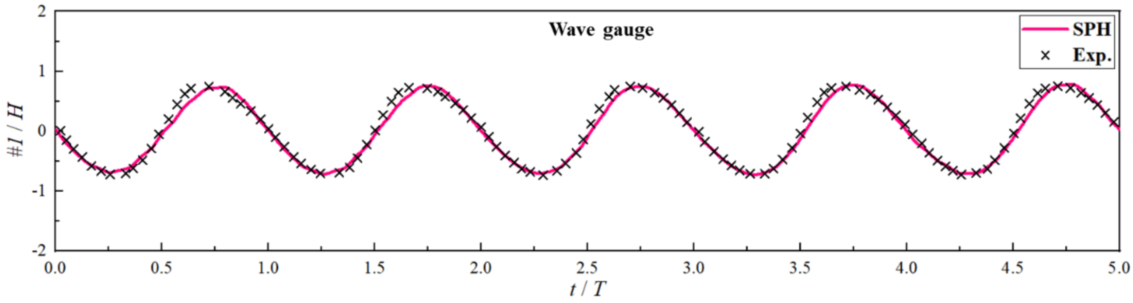

Fig. 5. Comparison of the experimental and modeled wave surface elevation

Furthermore, Fig.7 provides the comparison of the pontoon mooring loads between the numerical and experimental results. It can be observed that the two curves match well with each other, only a slightly underestimation of the maximum mooring amplitude occurred at one of the dual peaks of the mooring tensions. Likewise, the convergent mooring loads are in good agreement with the experimental data, which demonstrates that the developed numerical model successfully implement the simulation of the mooring system for a floating body.

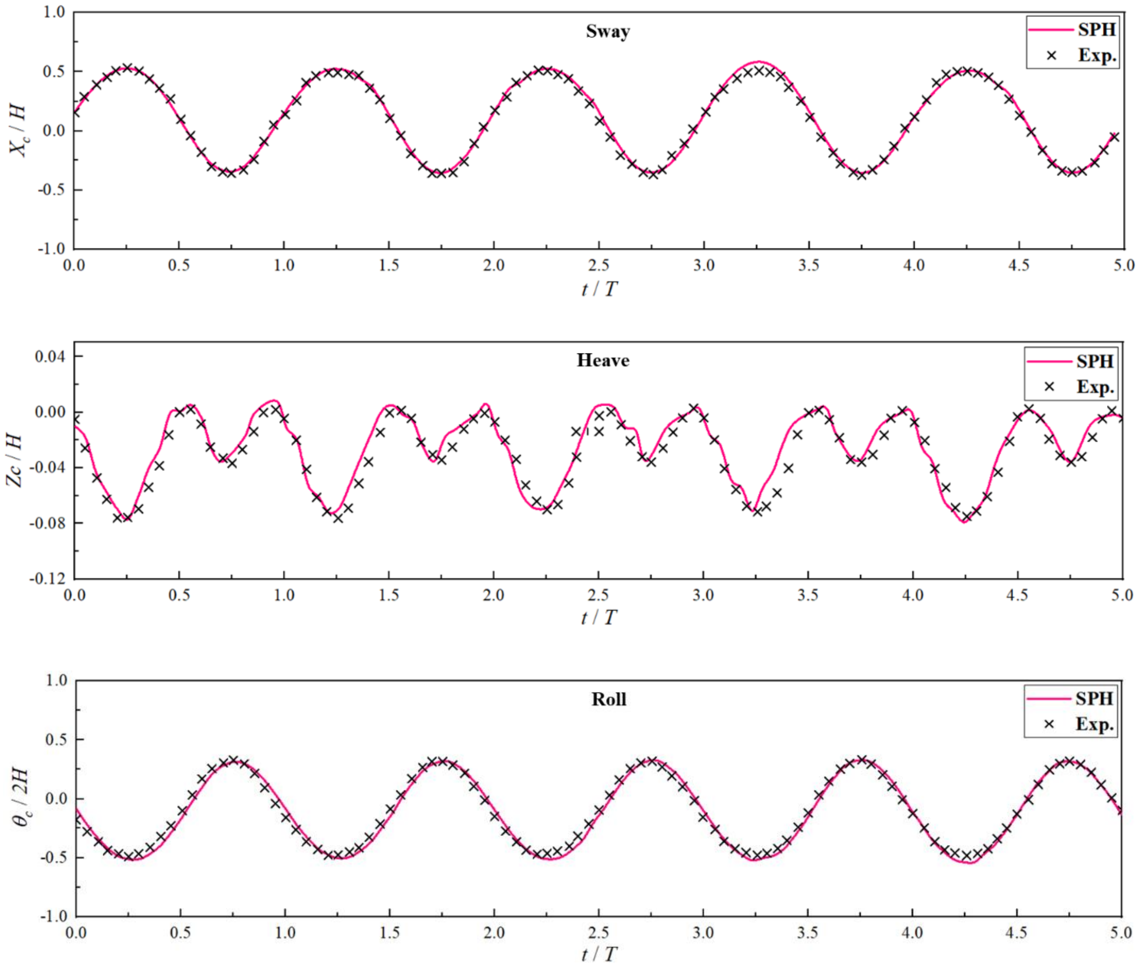

Fig. 6. Comparison of the experimental and modeled motion response of the pontoon buoy

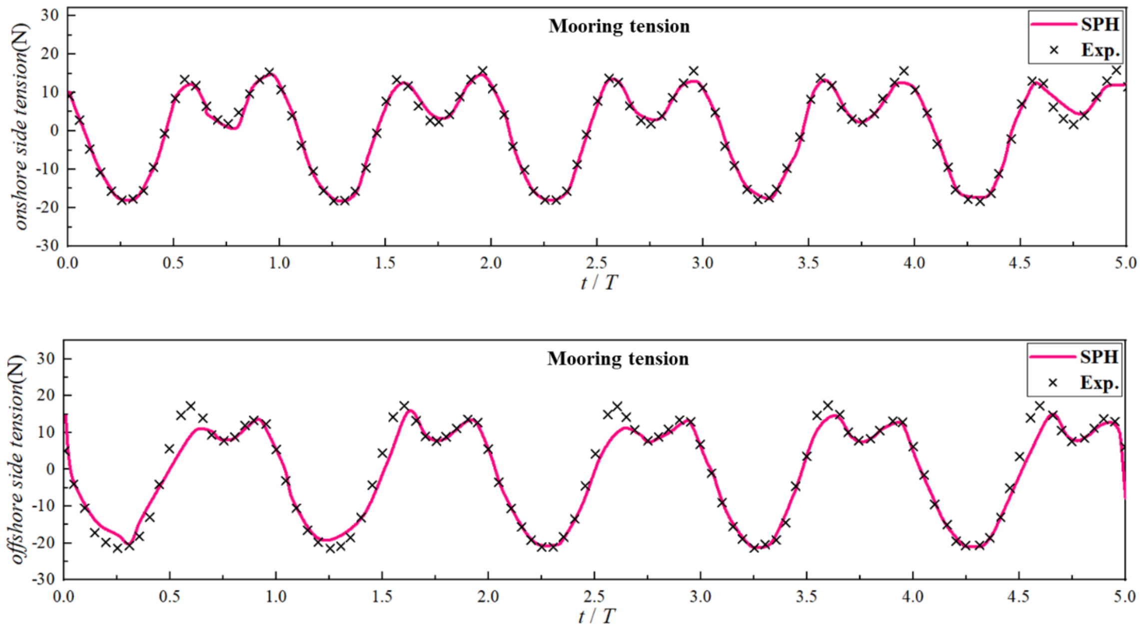

Fig. 7. Comparison of the experimental and modeled mooring loads of the floating body

3.3 Verification of immersing tunnel element with cable line

The process of the sinking of the tunnel element is critical and with highly safety requirements supported by the suspension cables. The accuracy of the modelling for the hoisting cable tension and the corresponding tunnel dynamics are very important in the modelling approach. Hence, in this section, the proposed submerged tunnel element lowering by suspension cable system is modelled and validated with the experimental results from Chen et al. (2009a). The experimental set-up of the carried out physical tank tests is shown in Fig.8, for the top view and the front view. The wave tank is 50 m in long, 3.0 m in width and 1.0 m in depth. The gravity and the negative buoyancy of the tunnel element are 1208.34N and 32.34N for a completely submerged state, respectively.

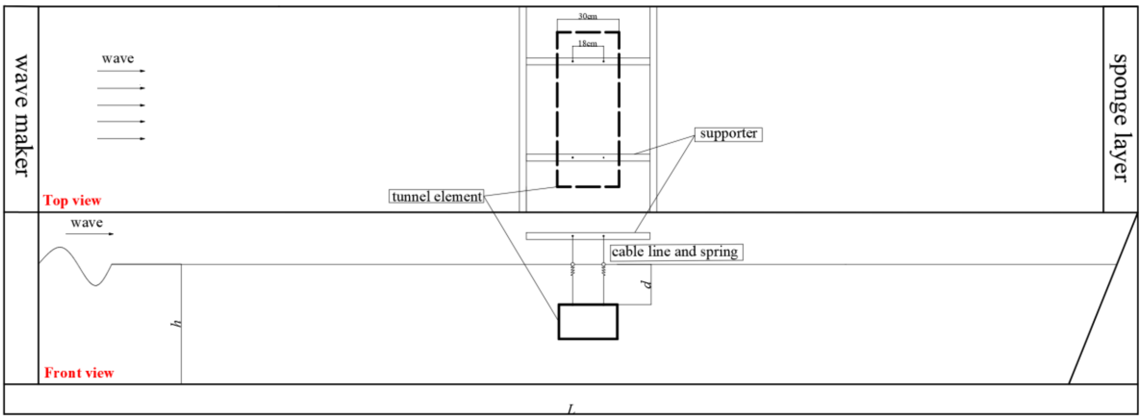

Fig. 8. Sketch of the experimental set-up for validation case

Fig.9 compares the modelled hoisting cable tensions of the tunnel element and the relative measured results obtained in the experiment, for case condition of H=0.03m and T=1.1s with the immersion depth of d=0.5m. Weightiness wire rope and light spring with stiffness are used for simulation in both the physical tank test and numerical model. From the validation results, the computed time history of the hoisting cable tensions matches well with the recorded data in the measurement. A slightly phase difference between the numerical and experimental cable tensions of the tunnel can be observed, which may be caused by the reflection effects acting on the tunnel in the physical tank tests. Therefore, the obtained good agreement between the modelling and experimental results on the dynamic motions, suspension cable force and mooring loads of the tunnel element proves the correctness and rationality of the developed SPH model, for simulating the tunnel-platform system proposed in this paper.

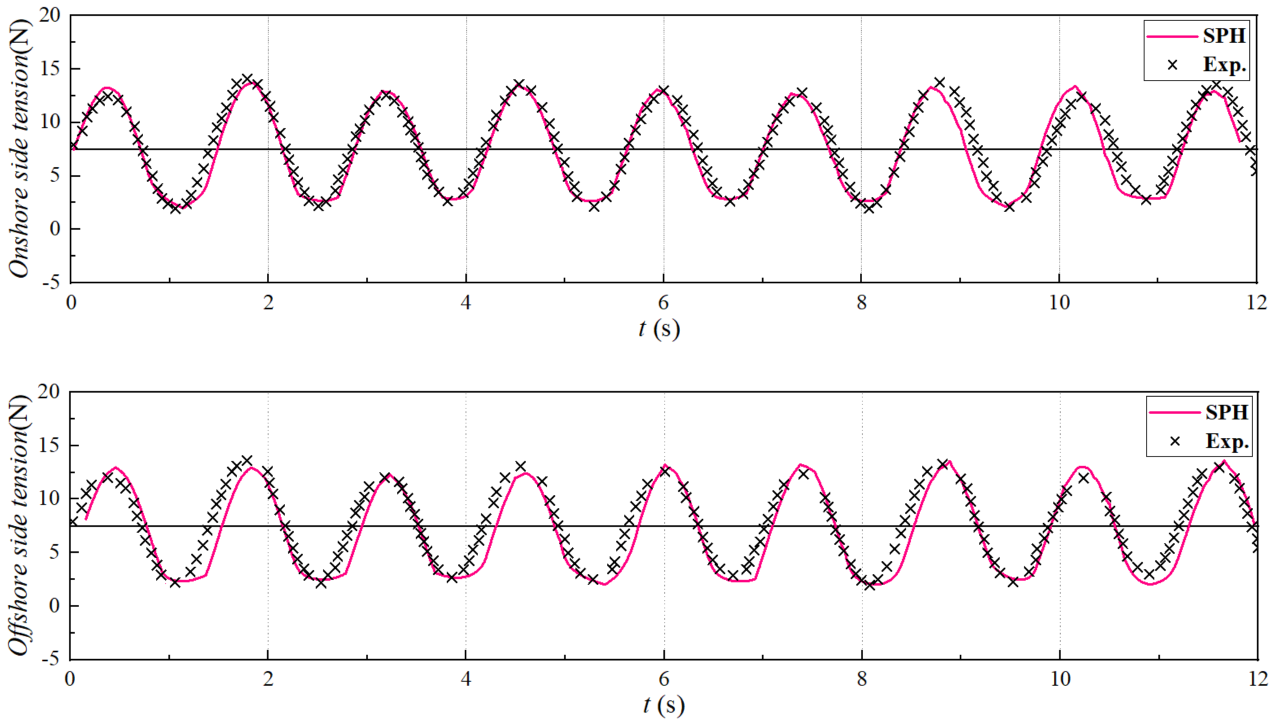

Fig. 9. Comparison of the experimental and modelled hoisting cable tensions of the tunnel-platform system

4. Results and discussion

In this section, the motion response of the tunnel element, the cable force and the mooring line tensions are analyzed. First, the three degrees of freedom of the tunnel motions are compared to the tunnel with and without mooring system. Then, the effects of the wave condition and the immersion depth of the tunnel on the motions and the mooring tensions are further analyzed and discussed. Finally, special attention is paid to the effect of mooring arrangement on the system dynamics and its mooring behavior. The results are discussed in detail below.

4.1 Effect of mooring system on the tunnel motions

Based on the regular wave tests in the modeling, the tunnel motion and the cable force of the coupled system are simulated to investigate the dynamic behavior of submerged affected by the mooring system. The sketch of the tunnel model suspended from a fixed platform is shown in Fig. 10 with two mooring conditions: a) without mooring lines; b) with mooring lines. For a better understanding of the dynamic behavior of the tunnel influenced by the mooring system, the normal positive incident wave is generated in the numerical model to observe the tunnel motions and its mooring tensions. The wave angle and the mooring angle with *z*-axis are fixed as α=90° and θ=30°, respectively, in this section.

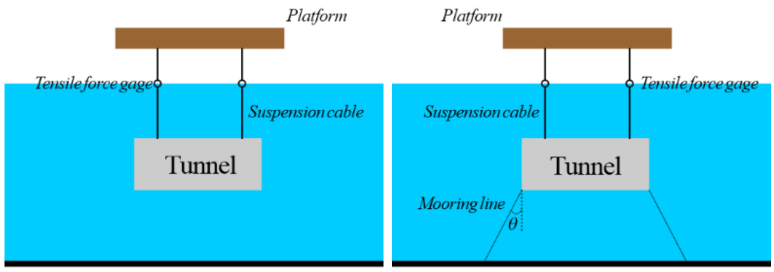

(a) (b)

Fig. 10. Model sketch of the tunnel element suspended from a fixed platform: (a) with mooring lines; (b) without mooring lines

Figs. 11-12 shows the numerical results of the motion response of the tunnel element and the corresponding suspension cable tensions within the selected test duration of approximately 10 regular waves. To evaluate the dynamic characteristics of the suspended tunnel and its mooring effects due to the resonance mode, the wave parameters are chosen to have the wave height of H=0.03m and the wave period close to the natural period of the tunnel-platform system of T=1.1s (without mooring), the immersion depth in this section is set as d=0.3m. The time history of the motion response of the tunnel element suspended from fixed platform is shown in Fig. 11. From the Figure, for the roll mode, it can be clearly seen that the motion amplitude of the tunnel element with mooring lines is obviously smaller than that of the tunnel without mooring lines. That is to say, after combining the mooring system, the tunnel roll motions are obviously constrained and sensitively affected by the mooring lines anchored at the seabed. However, the heave motion amplitude of the tunnel element performs an increasing trend after mooring. To explain this phenomenon, the synchronous suspension cable (hang the tunnel for sinking) tensions of the tunnel element are shown in Fig.12. It can be found that after combining the mooring system the suspension cable tensions getting increased at both the onshore and the offshore sides, this increasing cable tensions directly increases the inertia force acting on the tunnel, thus it motivates the motion response of the tunnel in heave mode. This phenomenon has also been observed in Ref Chen et al. (2009a) and the similar sinking case for tunnel-barge systems (Yang, 2017).

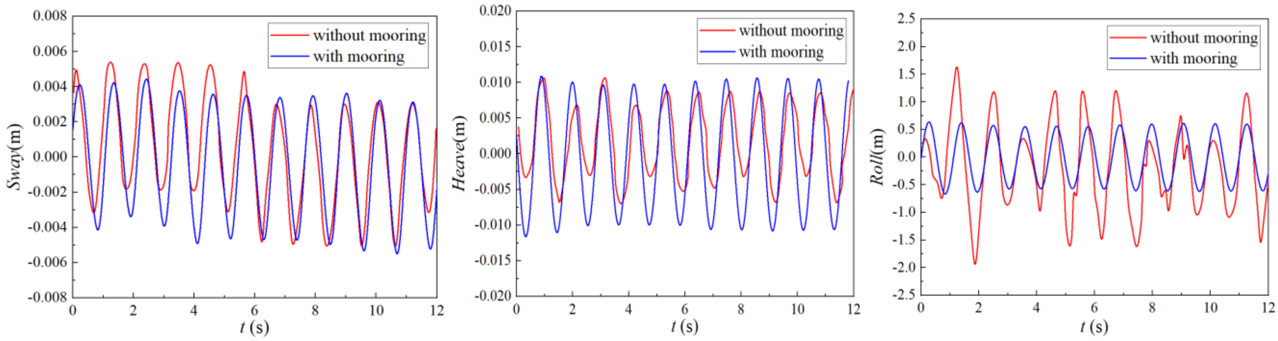

(a) (b) (c)

Fig. 11. Time history of the tunnel motions with and without mooring system (k_c=1.4x10^3 N/m)

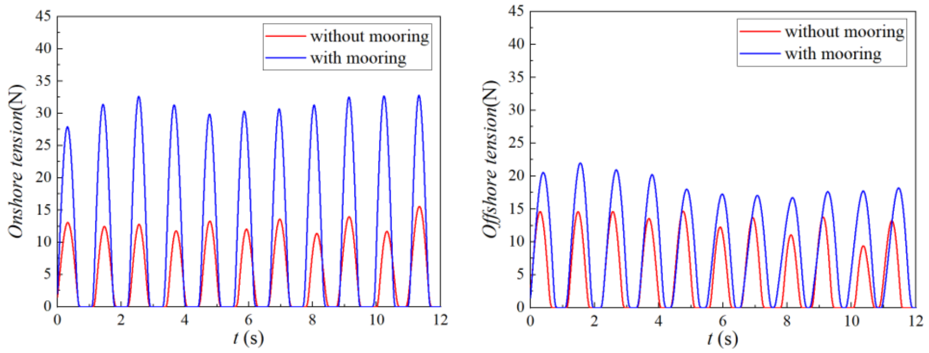

Fig. 12. Suspension cable tension of the tunnel with and without mooring lines (k_c=1.4x10^3 N/m)

Furthermore, the larger heave motion of the tunnel element would directly influence the safety sinking which is mainly controlled by the suspension cables. Thus, to reduce the tunnel motion response in heave, the larger stiffness of the suspension cables with k_c=5.8x10^3 N/m is chosen for comparison. The results of the tunnel motions and the suspension cable tensions with and without mooring liens are given in Fig. 13 and Fig. 14, respectively. In this case study, with the larger suspension cable stiffness (k_c=5.8x10^3 N/m), the mooring system could no longer motivate the inertia force of the tunnel, but only reduce the dynamic response of the tunnel itself in heave (Fig. 13 b). In Fig.14, for this case, the suspension cable tensions are apparently getting larger after combining the mooring system, and there is an obvious phase difference occurred between the two conditions (with and without mooring lines), compared with the case of k_c=1.4x10^3 N/m. The difference of the motion amplitudes between the two mooring conditions in the sway and roll modes is relatively small (Fig.13a and 13c). Based on the above analysis, to some extent, the suspension cables play a dominant role on controlling the tunnel heave motions, while the appropriate mooring configurations could help to restrict the tunnel motions for roll.

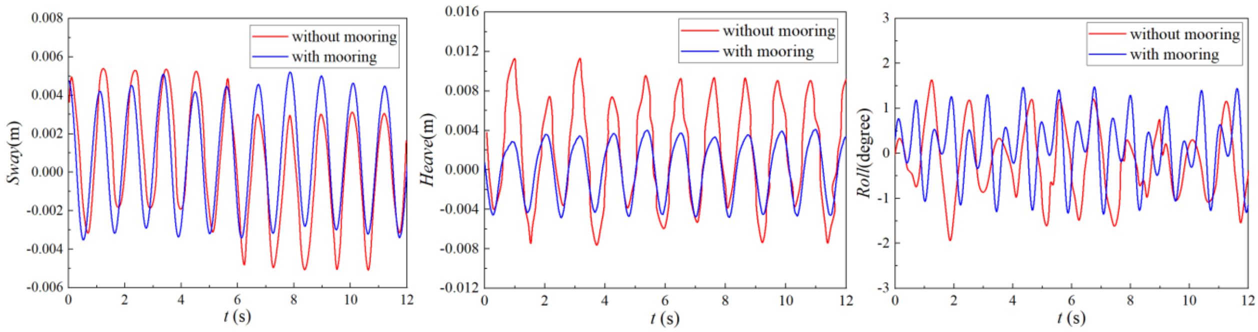

(a) (b) (c)

Fig. 13. Time history of the tunnel motions with and without mooring system (k_c=5.8x10^3 N/m)

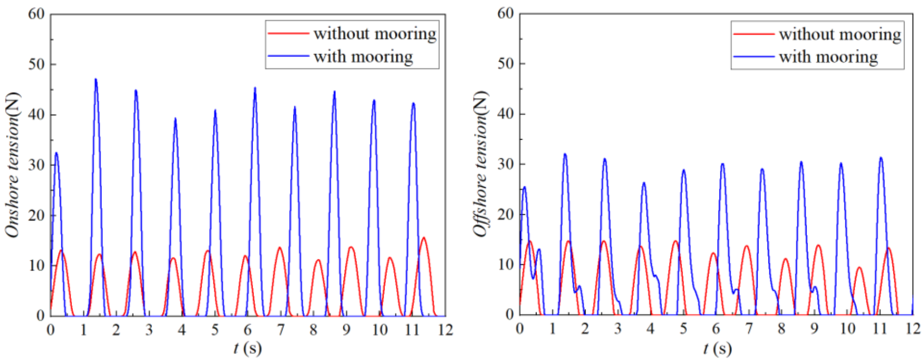

Fig. 14. Suspension cable tension of the tunnel with and without mooring lines (k_c=5.8x10^3 N/m)

4.2 Effect of wave parameters

The maximum and minimum motion amplitudes of the moored tunnel suspended from the platform are plotted in Fig. 15(a-c) under beam sea conditions T=1.1s and fixed immersion depth d=0.3m. Three different wave heights of H=0.03m, 0.04m and 0.05m are considered in the numerical model. In Fig.15(a-c), it can be clearly seen that the maximum tunnel motion amplitude increases approximately linearly with the increasing wave height, especially for heave mode (see Fig.15b). This is due to the tunnel experienced more severe dynamic response with the increment of the wave height, and thus leads to the stronger wave loads acting on the tunnel element. For heave, the downward motion amplitude is larger than the upward motion of the tunnel.

The motion amplitudes of the tunnel element against different wave periods are plotted in Fig.15(d-f). To be conservative, wave periods from 0.95s to 1.4s were chosen, to cover a range of the resonance conditions for this proposed model. For sway, the results clearly show an increasing trend of the tunnel motions with increasing wave period, for each different wave height conditions (see Fig.15d). For heave, the maximum motion amplitude of the tunnel increased with the increasing wave period until reach a local maximum at T=1.25s, and then decreased. However, for the roll motions, based on the increasing trend with the wave height and wave period, the local peak(T=1.15s) and the trough(T=1.25s) of the tunnel motions can be concurrently observed, which indicates that multiple resonant mode would be happened during the sinking in roll.

Combining the effects of wave height and wave period, Fig.15 (g-i) present the percentage difference of the tunnel motion response against the wave condition of H=0.03-0.05m and T=0.95s-1.4s with the immersion depth of 0.3m. Whereby the percentage difference $\Delta\eta$ is obtained as follows

$$\Delta\eta = \left(\left(\eta_{h2}-\eta_{h1}\right)/\eta_{h2}\right)\times 100\% \tag{33}$$

From Fig.15(g-i), it is clearly shown that the maximum motion percentage difference between the wave height of 0.05m and 0.03m is larger than the other one, for sway, heave and roll modes. Compared with the roll mode, the percentage difference between the wave height of 0.05m and 0.03m is relatively larger, nearly reach two times of the percentage for comparison between H=0.03m and H=0.04m. Furthermore, the maximum motion percentage difference increased nonlinearly with the increment of the wave heights, especially for the longer waves, i.e. T>1.15s. This is probably because of the resonance mode occurs at this range of wave period, which made the effect of wave height significantly during its sinking process under such combined wave conditions.

a *d* *g*

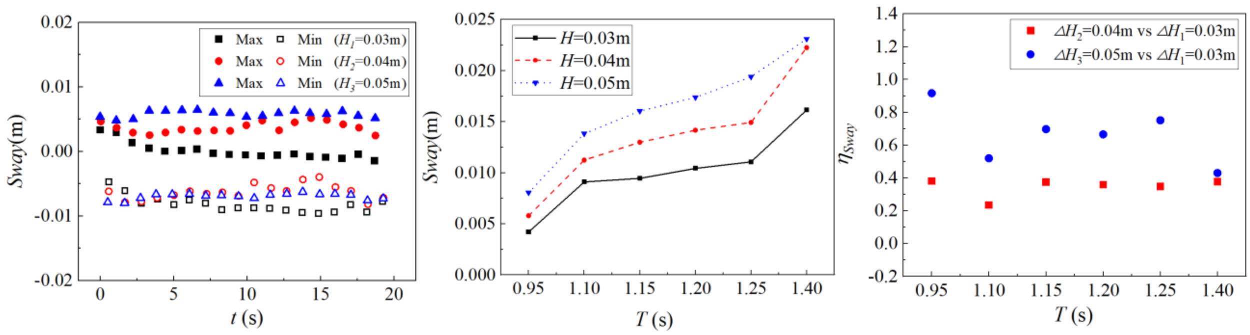

b *e* *h*

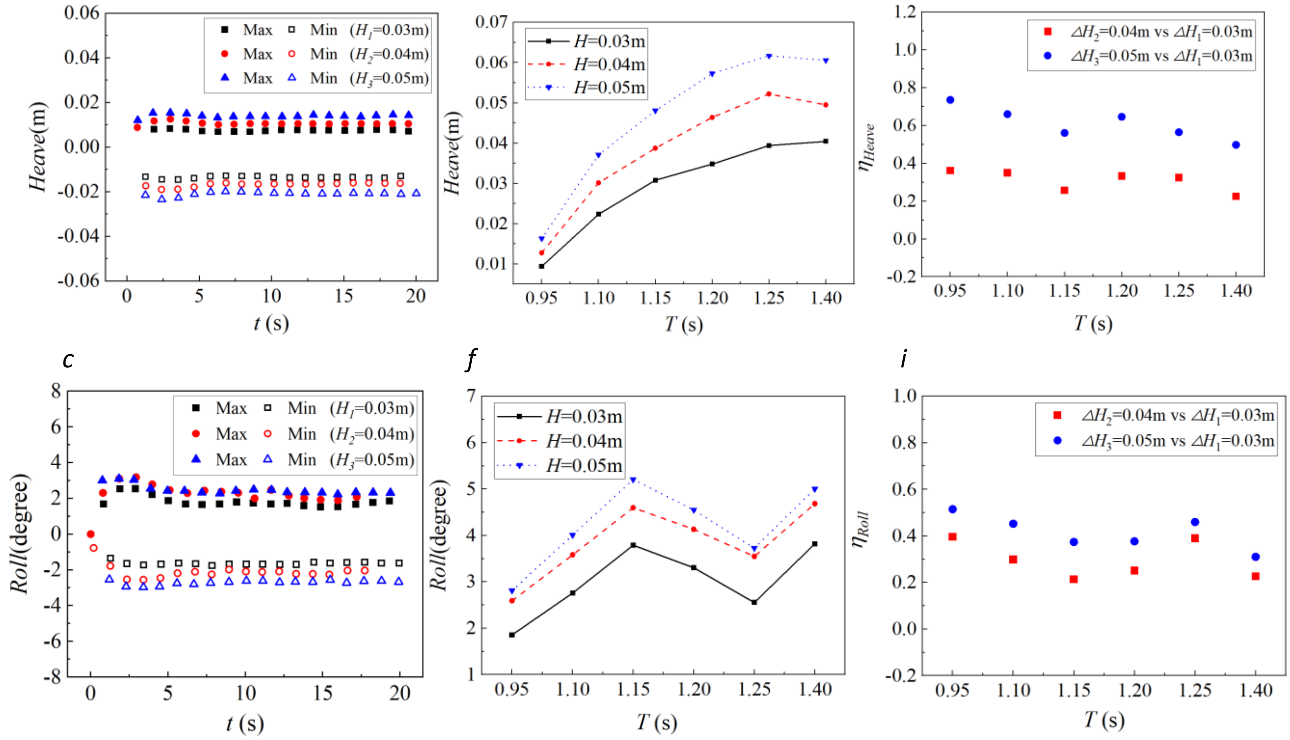

Fig. 15. Motion response amplitude of the tunnel element for different wave heights

The comparison of the mooring tension of the tunnel between three different wave heights (H=0.03m, 0.04m and 0.05m) with wave period of T=1.1s are shown in Fig.16. The results show that the suspension cable tensions increase with the increasing wave heights, the offshore side cable tensions perform an approximately linear relationships with the increment wave height, whist the onshore side cable tension increases more nonlinearly because of the complicated fluid-structure interactions occurring at the wave-facing zone of the coupled tunnel-platform system. This phenomenon can be also observed in the mooring line tensions of the tunnel that is drawn in Fig.17. Besides, it can be observed that the onshore tensions of the suspension cable are larger than that of the offshore suspension cable for each wave height case, which are also obtained in the numerical results for different wave period conditions, as is shown in Fig.18(a). In Fig. 18(a) and (b), for both the onshore(offshore) suspension cable and mooring tensions, the cable/mooring tensions increase with the increasing wave period until reach a local maximum at T=1.25s, and then decrease. This local peak period is related to its natural period of the system, which caused by the stiffness of the suspension cable and mooring lines set in these model cases. Different with the suspension cable, the mooring tension at the offshore side performs an increasing trend after the local peak resonant wave period, which may be due to the constrained motions controlled by the cable force resistance mechanism, for larger dynamic motion modes of the tunnel.

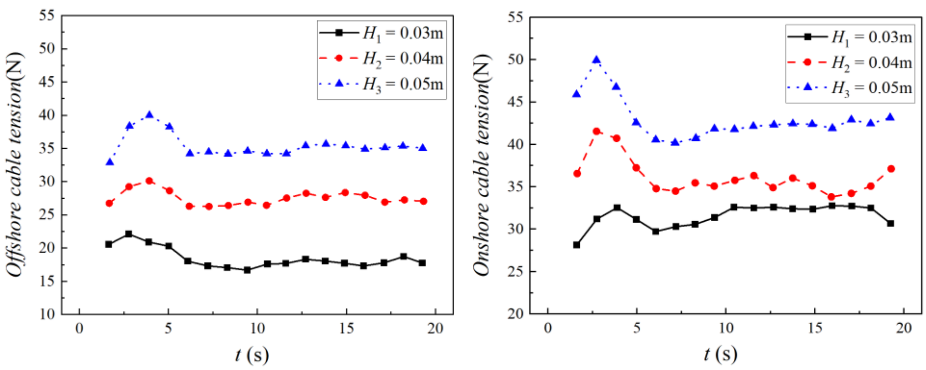

Fig. 16. Suspension cable tensions of the tunnel-platform system for different wave heights

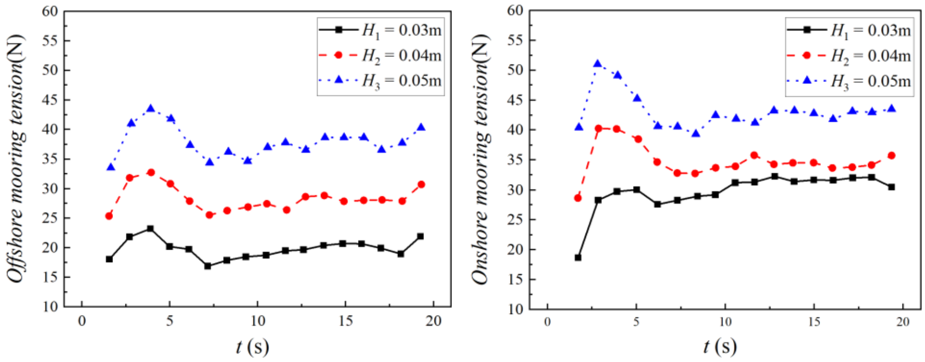

Fig. 17. Mooring tensions of the tunnel-platform system for different wave heights

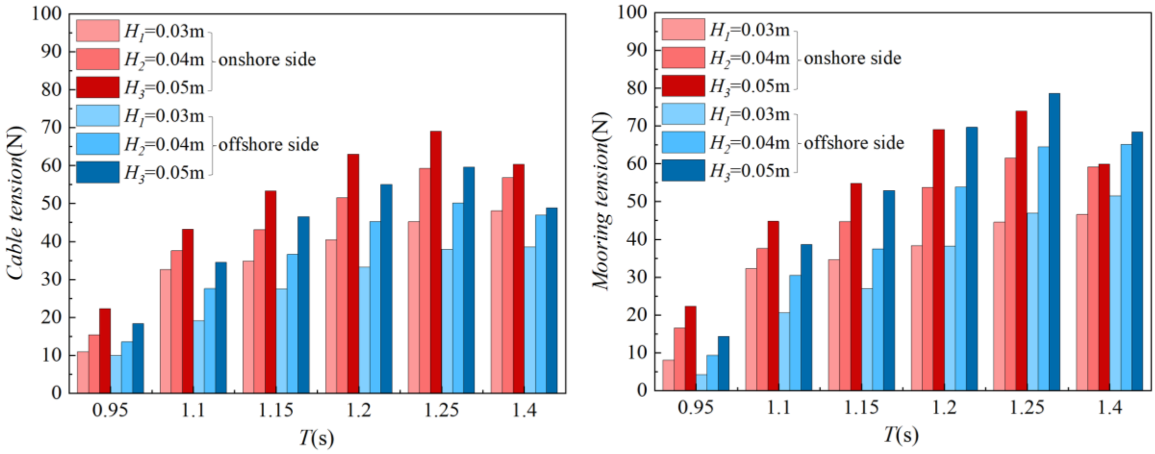

(a) (b)

Fig. 18. Comparison of the suspension and mooring tensions of the tunnel-platform system with different wave periods

4.3 Effect of sinking depth of the tunnel

In this section the motion response and the cable tensions of the moored tunnel with different sinking depth are investigated. Three different sinking depth of the tunnel element suspended from the platform are considered, they are *d*=0.3m, 0.4m and 0.5m. The corresponding ratios of the sinking depth and the water depth are 0.375, 0.5, and 0.625. The wave periods of *T*=0.95-1.4s are chosen to evaluate the effects of the sinking depth of the tunnel. Figs. 19a-f show the motion amplitudes of the tunnel element as well as the percentage difference for a range of wave periods and for different sinking depths with wave height of *H*=0.03m. The percentage difference $\Delta\eta$ is calculated using equation(33), where the sinking depth *d*=0.3m is used as reference case. The tunnel motion amplitudes are simulated for sway mode (19a), heave mode(19b) and roll mode(19c). The corresponding presentations of percentage differences are given in Figs. 19d-f, respectively. It can be seen from Fig.19 that the motion amplitudes of the moored tunnel increase with a decrease of the sinking depth of the tunnel, allowing nearly linear growth with the decreasing sinking depth in heave. In Figs. 19d-f, the maximum and minimum of the percentage difference for the sway motion $\Delta\eta\_sway$ between *d* = 0.4m and 0.3m is 23.5% and 38.1%, respectively. Whilst the $\Delta\eta\_sway$ between *d* = 0.5m and 0.3m is of the order of 51.9% and 91.6%. The heave mode is increasing for larger wave periods. The negative percentage difference $\Delta\eta$ presents a decrease in the motion response of the tunnel. The percentage difference $\Delta\eta\_heave$ are at the order of -69.1% to -47.5% (*d* = 0.4m vs 0.3m) and -46.5% to -20.3% (*d* = 0.5m vs 0.3m), respectively. As for the roll mode, for the local peak period corresponding to the maximum percentage difference occurs at the wave period of *T*=1.2s. The percentage difference for roll between *d*=0.4m and 0.3m is at a smaller magnitude compared to the sway and heave mode ($\Delta\eta\_roll$ = -16.7% to -5.1% (*d* =0.5 vs 0.3m)), whilst another case in the roll mode is of $\Delta\eta\_roll$ = -45.1% to -10.5% (*d* = 0.4m vs 0.3m).

Furthermore, the force behavior of the suspension cables and the mooring system of the coupled platform-tunnel are discussed under different sinking depth of the tunnel. In Fig.20, the suspension cable tension and the mooring line tension of the tunnel decrease with the increase of the sinking depth, for both the onshore side and the offshore side cables. From Fig.20(a), it can be observed that the onshore suspension cable tensions are slightly larger than that of the offshore side one, with each different wave period condition. While, for the mooring system, the line tension variates little between the onshore and offshore cables, experiencing almost the same dynamic process under the combined wave period and sinking depth impacts, as can be seen in Fig.20(b).

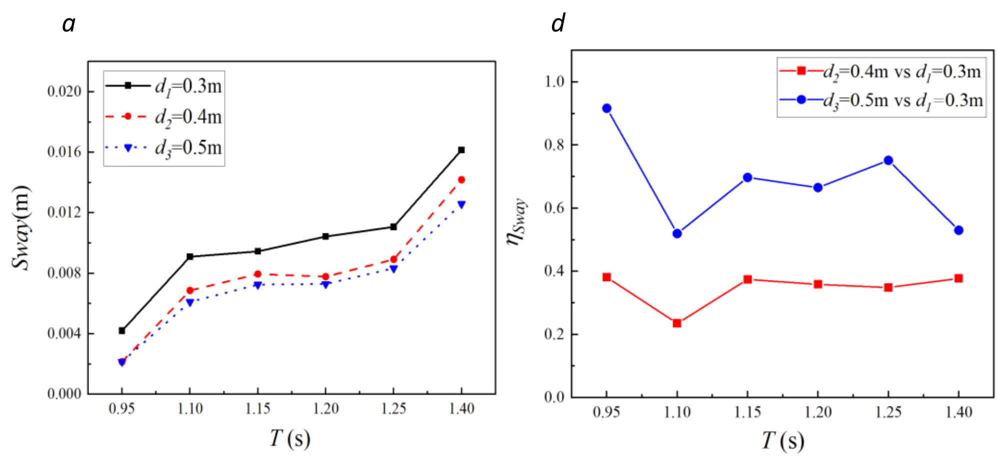

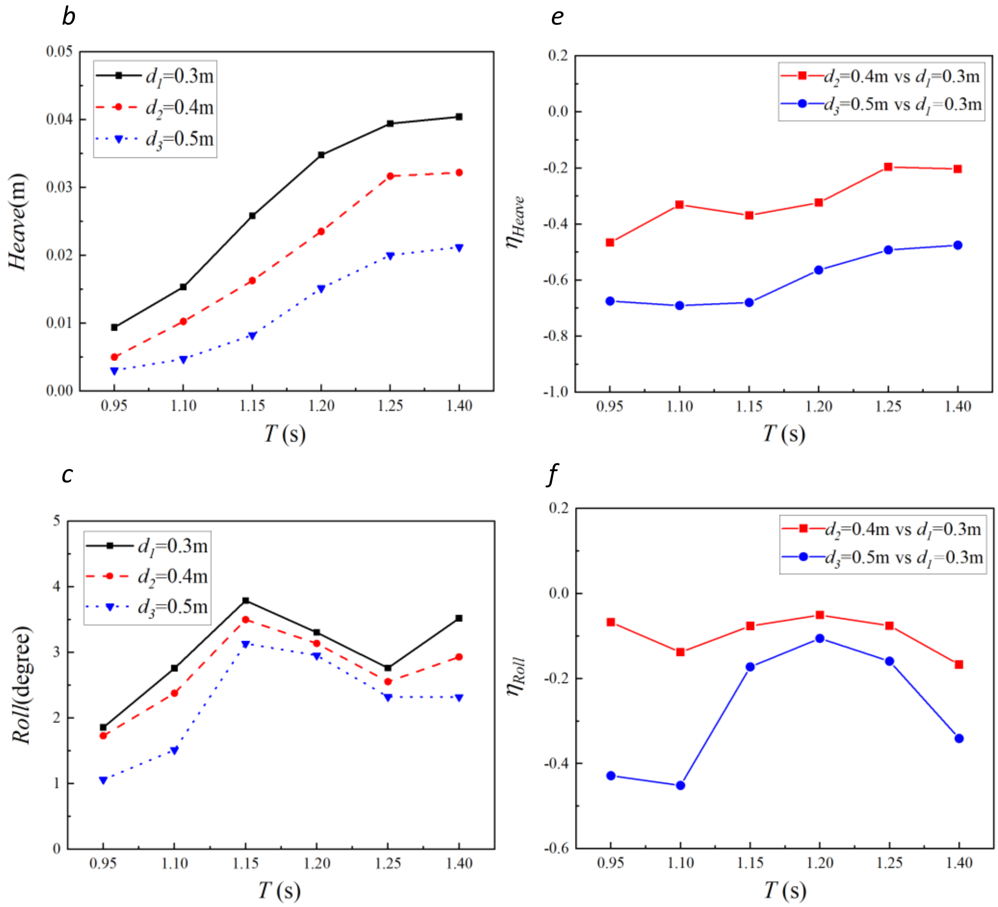

Fig. 19 a-f. The maximum motion amplitudes of the moored tunnel with different sinking depths and H = 0.03m: a) sway motion, b) heave motion, c) roll motion, d) – f) corresponding percentage difference $\Delta\eta\_sway$, $\Delta\eta\_heave$, $\Delta\eta\_roll$

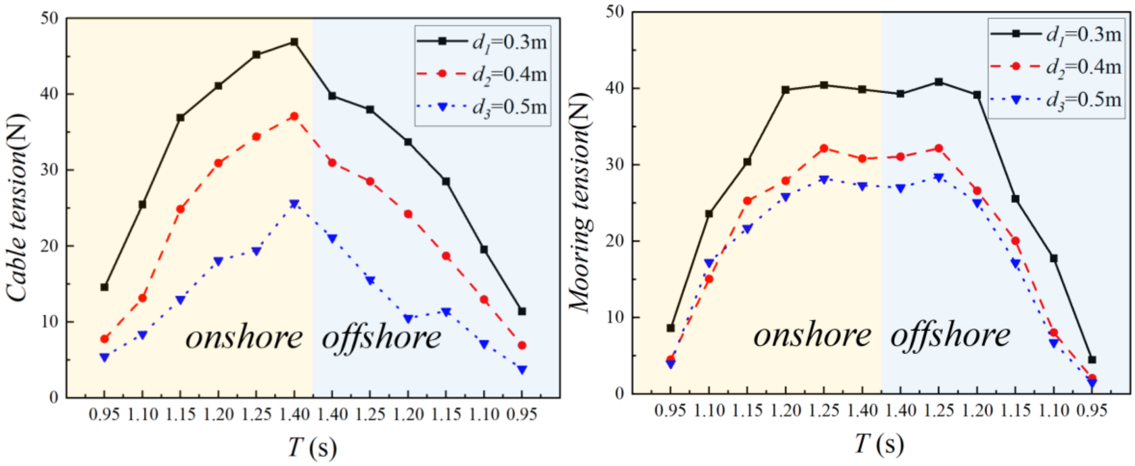

(a) (b)

Fig. 20. The maximum suspension cable force and mooring tensions of the tunnel for different sinking depths

4.4 Effect of mooring configurations

In order to investigate the mooring behavior effects on reducing the dynamic response of the tunnel element suspended from a fixed platform, the mooring configurations such as the mooring angle and the mooring stiffness of the chain are involved in this model study to better understand the restricted behavior of the mooring system. The schematic of the mooring arrangement of the tunnel element was set and represented in Fig. 21(a-d). Due to the different arrangement of the mooring lines (the mooring angle variated in *x-z* coordinate plane), the tunnel element was anchored by the mooring lines which were set along the y-axis. As is shown in the Fig.21, four mooring angles of the tunnel element are considered in the modelling, the incident wave angle is fixed as α=90° with *z*-axis as the numerical set-up above.

Firstly, the mooring behavior of the tunnel element with the four mooring arrangement is simulated. Figs.21(e-h) show the dynamic history of the mooring tensions for the onshore and offshore side cables. The mooring angle θ here is defined as the acute angle between each mooring line and *z*-axis. It can be found that the phase difference between the onshore and offshore mooring tensions decreases with the decreasing mooring angle (the mooring angle is defined with *x*-axis). For the mooring angle greater than or equal to 45°, the offshore mooring tension is lower than that of the onshore side one. For θ ≥45°, the percentage difference of the mooring tension amplitude increases with the increasing mooring angle. While for θ=30°, the mooring tensions at the onshore and offshore sides are close to each other. Among the four mooring arrangements of the tunnel, the maximum tension of the mooring line occurs at the condition of θ=60°, whilst the smallest mooring tension occurs at θ=75°. And the mooring tensions between the mooring angle of θ=30° and θ=45° are less differentiating at some level. Correspondingly, in the coupled system, the force of the suspension cables induced by the tunnel response and mooring loads are also investigated, the relevant results for the same condition above are shown in Figs.21(i-l). It shows that the suspension cable and the mooring lines are almost in the anti-phase, especially for the smaller mooring angle cases. For heave, the suspension cable force is larger than the

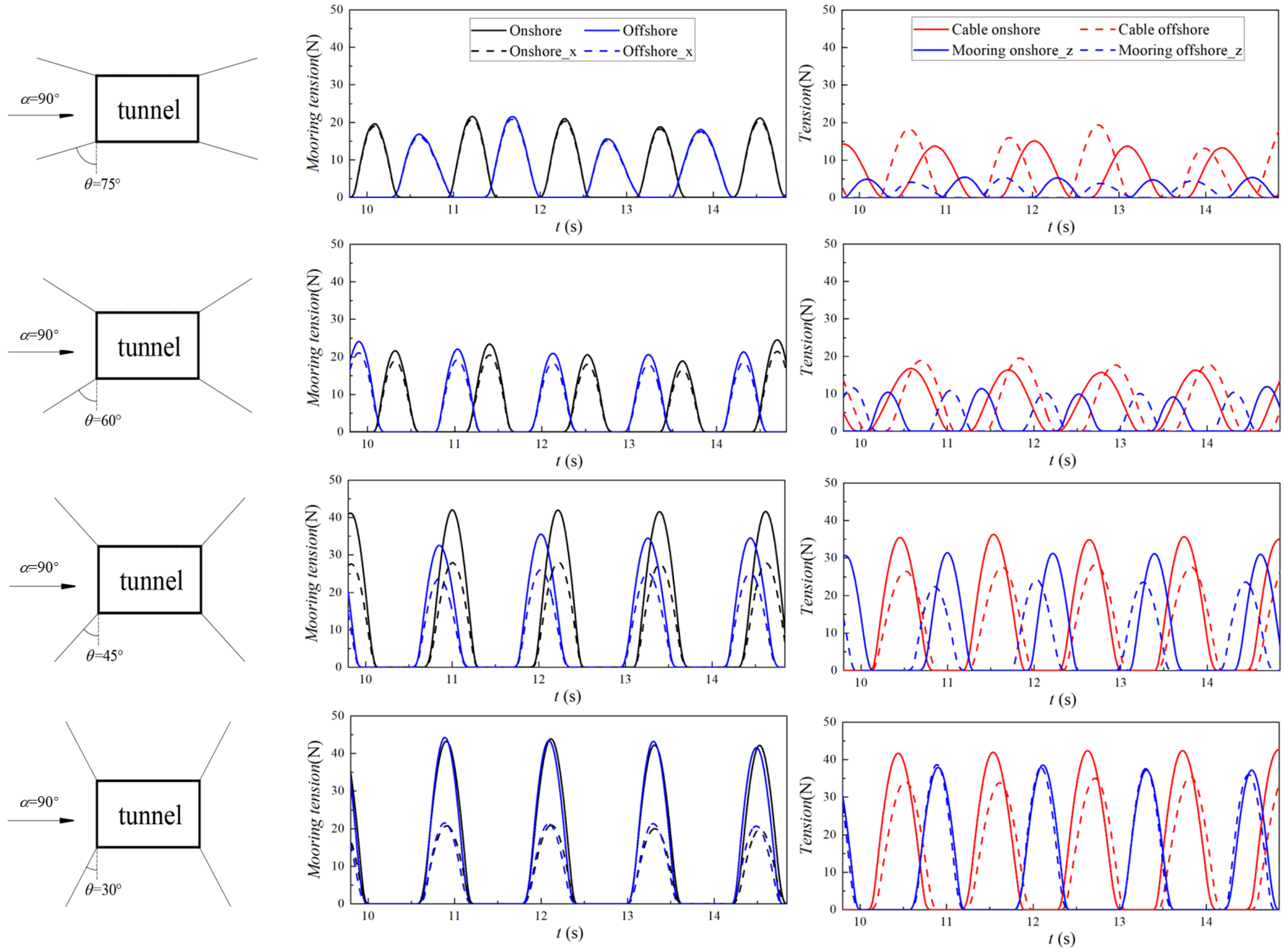

Fig. 21. Dynamic behavior of the mooring and suspension cables with four different mooring arrangement: a-d) tunnel mooring arrangement types; e-h) time history of the mooring tensions; i-l) time history of the suspension cable tensions

mooring tension component of the tunnel in *z* direction, at the cases for larger mooring angles (θ=75° and θ=60°). It illustrates that the mooring angle can affect both the mooring line tension and the suspension cable force, the cable loads perform an increasing trend with the decrease of the mooring angle of the tunnel element.

Then, the amplitude response of the tunnel with the above four mooring arrangements against three typical wave periods (T=0.95s, 1.1s and 1.2s) are obtained and shown in Fig.22. Here, two different mooring stiffness with k_m=3.4×10^{3}N/m and k_m=7.4×10^{3}N/m are both considered, to evaluate the restraint behavior of the mooring system on the tunnel motions in sway, heave and roll modes. Fig.23 and Fig.24 show the scalar filed of the pressure and the velocity around the tunnel, with the selected cases of θ=75° and θ=30° (for two mentioned mooring stiffness) during two wave period. This series of the motion amplitudes of the tunnel element were simulated with a range of tests under regular waves. In the sway and roll modes, it can be seen from Figs.22(a) and (c) that the motion response of the tunnel element increases with the increasing mooring angle in this range of the numerical tests, whilst for heave the tunnel motion performs an inversely trend that it increases with the decreasing mooring angle (see Fig.22(b)). Comparing the flow pressure with the flow velocity simulated at the same period, it can be seen that the pressure in the flow field around the tunnel variated stronger for the larger mooring angle case of θ=75°, generating more local contaminating field of velocity at the tunnel edge corners, as can be seen in Fig.23 and Fig.24, respectively. That is to say, for this proposed specific tunnel-platform system, the smaller mooring angle could reduce the dynamic response of the tunnel in sway and roll modes, but would help to increase the inertia force of the tunnel under such combined suspension-mooring controlled system.

The effect of the stiffness of the mooring lines is also conducted to further investigate the motion restricting mode. The numerical results show that the tunnel motion response reduced by the larger mooring stiffness, in sway and roll directions for all mooring line angles 30-75°. While for heave the mooring stiffness effect on the motion response of the tunnel is little, only show a slightly decreasing trend with larger mooring stiffness at cases of θ = 30-60°, for wave period of 0.95s and 1.1s. As can be observed in Fig.23 and Fig.24, for larger mooring stiffness of k_m=7.4×10^{3}N/m at the condition of smaller mooring angle, there is almost no vortex shedding and the pressure field is uniformed which could be owing to the well restricted performance of the suspension-mooring system for certain incident waves. Generally, for the coupled mode of the suspension-mooring system of the tunnel, the mooring system plays a role on reducing the tunnel roll motion and the sway low-frequency motion, the larger mooring stiffness with the smaller mooring angle (with *z*-axis) is more reliable and could help to improve the motion restriction effects, from the point of view on reducing the mooring operational risks. The heave dynamic response of the tunnel element is mainly controlled by the suspension cables, even though the tunnel has a relatively larger mooring stiffness to a certain extent. Therefore, a point needs to be point out is that the single mooring tensions or the suspension cable forces cannot be only used to evaluate the support capability of the tunnel element, for different method using in the submerged installation (including different vessel type), the optimal mooring system arrangement needs to be individually studied and determined in conjunction with the coupled motion modes for design.

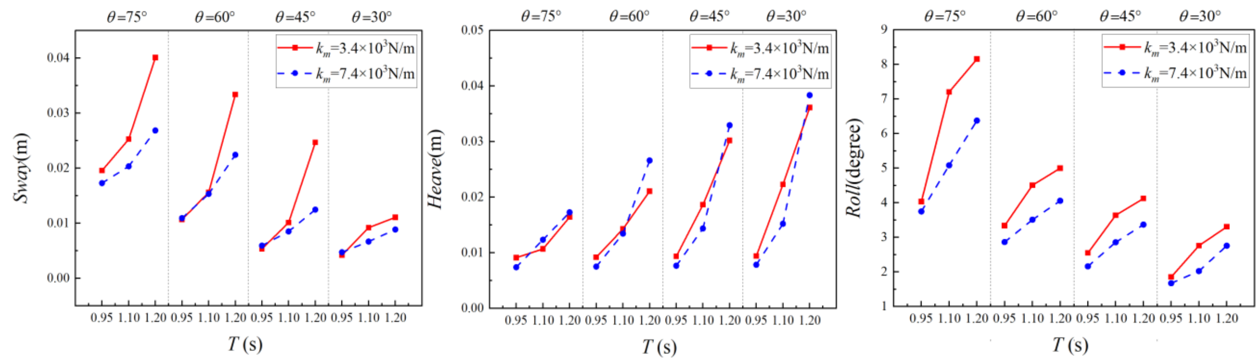

(a) (b) (c)

Fig. 22. Comparison of the tunnel motions with different mooring angles and different mooring stiffness: a) sway; b) heave; c) roll

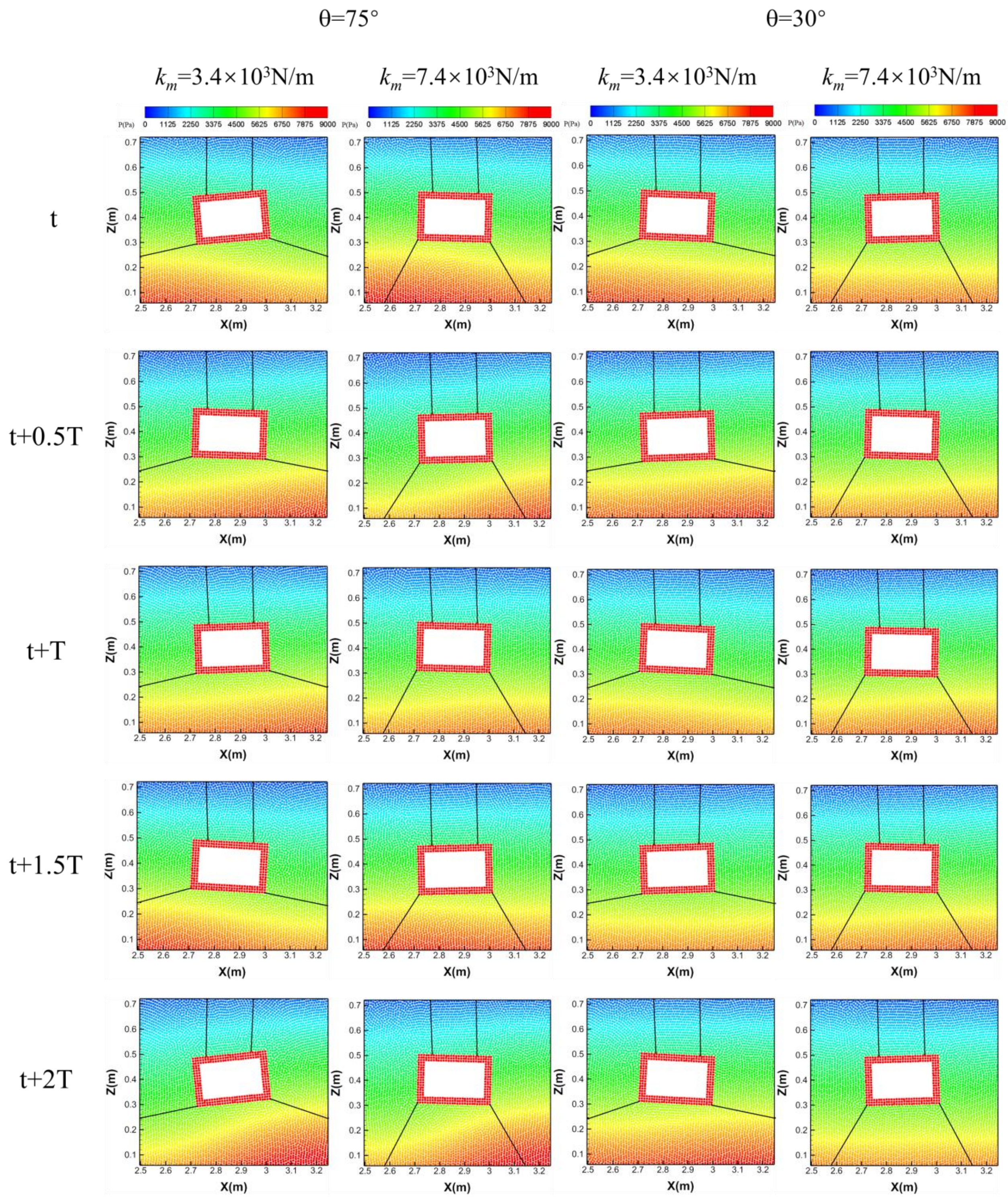

Fig. 23. Scalar view of the pression field around the tunnel element support by the suspension cable and mooring system.

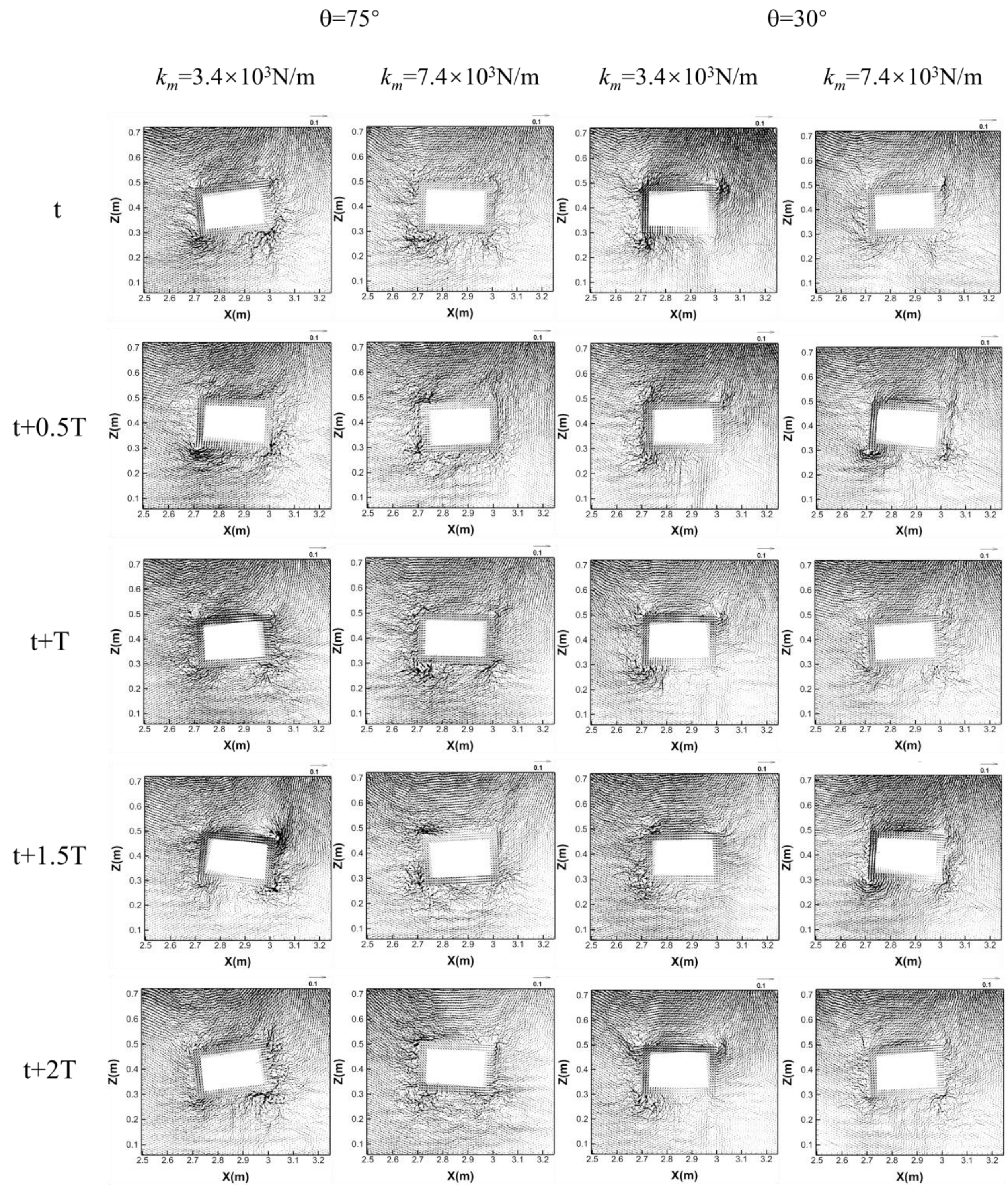

Fig. 24. Scalar view of the velocity field around the tunnel element support by the suspension cable and mooring system.

5. Conclusions and Future work

In this paper, a numerical model for a submerged tunnel element suspended from a fixed platform is developed by using SPH method, the additional mooring system of the tunnel was investigated to improve the understanding of the coupled dynamic response of the tunnel induced by the multiple cable force actions subjected to waves. The modelling results of the tunnel motions, the cable forces and the mooring loads of the combined system were compared with the measured data for numerical validation at experimental scale. Based on the numerical modelling, the effects of the wave characteristics and the mooring configurations on the complicated dynamics of the submerged tunnel suspended from a platform were discussed.

The obtained results in this study demonstrate that the additional mooring system used to support the submerged tunnel during its installation procedure introduces an important aspect in the tunnel dynamic behavior, which needs to be considered in the early design for tunnel sinking. The comparison results illustrate that the mooring system plays a key role on reducing the tunnel motions in roll and sway (low-frequency mode), but the heave motions are mainly controlled by the suspension cables. Therefore, it is crucial that consideration is made on how to limit or control the inertia force of the tunnel-platform system that caused by the additional tunnel moorings. Determining which suspension cable stiffness and mooring arrangement can be classed as safe for sinking, could help to avoid the excessive dynamic response of the tunnel that inducing the cable breakage during installation at an early design stage.

The maximum suspension cable tensions and tunnel mooring loads increase with the increment of wave height as well as the decreasing sinking depth of the tunnel. The amplitude tensions of the mooring system increase with the wave period until reached a local maximum at T=1.15-1.25s (for sway, heave, and roll) and then occurs a decreasing trend. The onshore tensions of the suspension cable are larger than that of the offshore side one. The largest tunnel motions and the lowest mooring tensions both occur at condition of θ=75°. However, the lowest motion response of the tunnel element occurs when the mooring angle is set as θ=30°, whilst the largest tension on the mooring lines occurs at θ=60°. Hence, evaluation of the mooring system effects needs to be considered in conjunction with the suspension cable behavior and the coupled tunnel-platform dynamic responses, the mooring line arrangement should be identified and determined to reduce the operational risk during tunnel lowering.

Overall, this numerical model presented here has its limitations that it is a 2-D WCSPH model and the tunnel lowering process is specific as discontinuous certain immersion depth under the water. Therefore, further work should be conducted: 1) optimization of the mooring system (coupled with suspension cables) in a 3-D numerical model to investigate the fully dynamic tunnel motions in long-term real sea conditions, aiming to find an appropriate support cable arrangement for motion restriction of lowering the tunnel; 2) studies of continuously lowering of the tunnel element by using SPH method, and consequently develop a numerical model for simulating a tensible lowering support system during installation.

Acknowledgement

This paper is financially supported by the National Natural Science Foundation (Grant No.52101306), the National Science Foundation of Shandong Province (Grant No. ZR2021QE121), the Fundamental Research Funds for the Central Universities (Grant No. 3072022JC2701), National Science Foundation of Heilongjiang Province (Grant No. LH2021E049), the Open Foundation of State Key Laboratory of Coastal and Offshore Engineering of Dalian University of Technology [LP2006], the British Council (BRI JOINT project) and EPSRC ResIn project (EP/R007519/1) who part funded the corresponding author, and the China Scholarship Council (award to Yang Can for study abroad at the University of Exeter). Special thanks go to the anonymous reviewers for their careful reading of the manuscript and valuable comments.

References

A. J. C. Crespo, M. Gómez-Gesteira, R. A. Dalrymple, 2017. Boundary Conditions Generated by Dynamic Particles in SPH Methods. Computers Materials Continua 5, 173—184.

A. Glerum, 1995. Developments in submerged tunnelling in Holland. Tunnelling and Underground Space Technology 10 (4), 455-462.

Aono, T., Sumida, K., Fujiwara, R., Ukai, A., Yamamura, K., Nakaya, Y., 2003. Rapid stabilization of the submerged tunnel element. In: Melby, J.A. (Ed.), Proceedings of the Coastal Structures 2003 Conference Portland, Oregon, August 26–30, 2003. American Society of Civil Engineers, pp. 394–404.

Bouscasse, B., Colagrossi, A., Marrone, S., Antuono, M., 2013. Nonlinear water wave interaction with floating bodies in SPH. J. Fluids Struct. 42, 112-129.

Can Yang, Sam D. Weller, Yong-xue Wang, et al. Hydrodynamic response of a submerged tunnel element suspended from a twin-barge under random waves[J]. Ocean Engineering, 2017, 135:63-75.

Chen, K.Q., Peng, S., Wu, W.G., et al. Model test of immersed tunnel element in towing flume in winds, waves and currents[C]. Twenty-second Int. Offshore Polar Eng. Conf., 2012:831-836.

Chen, Z.J., Wang, Y.X., Wang, G.Y., Hou, Y., 2009. Experimental investigation on immersion of tunnel element. In: 28th International Conference on Ocean, Offshore and Arctic Engineering, Honolulu, Hawaii, America. OMAEn 2009–79073.

Chen, Z.J., Wang, Y.X., Wang, G.Y., Hou, Y., 2009b. Frequency responses of immersing tunnel element under wave actions. J. Mar. Sci. Appl. 8 (1), 18–26.

C. Altomare, J.M. Domínguez, A.J.C. Crespo, J. González-Cao, T. Suzuki, M. Gómez-Gesteira, P. Troch, 2017. Long-crested wave generation and absorption for SPH-based DualSPHysics model, Coastal Engineering 127, 37-54.

Dalrymple, Robert, Knio, Omar, 2001. SPH modeling of water waves. Proceedings of coastal dynamics 2001 260:779-787.

Fu, Q.G., 2004. Development and prospect of submerged tunnels. China Harb. Eng. 2004 (5), 53–58.

Hirakuchi Hiromaru, Kajima Ryoichi, Kawaguchi Takashi, 1990. Application of a Piston-Type Absorbing Wavemaker to Irregular Wave Experiments. Coastal Engineering in Japan 33, 11-24.

Huang, G.X., Song, Y., Sun, Z.X., et al., 2019. Experimental investigation on the coupling between immersion rig and tunnel element during freeboard elimination. Ocean Eng. 186, 106068.

Ingerslev, L.C., Fasce, P.E., 2012. Innovations in resilient infrastructure design: submerged and floating tunnels. Proc. Inst. Civ. Eng. 165 (6), 52.

Janssen, W., Haas, P.D., Yoon, Y.H., 2006. Busan–Geoje Link: submerged tunnel opening new horizons. Tunn. Undergr. Space Technol 21 (3), 332–332.

J.J. Monaghan, 1985. Particle methods for hydrodynamics. Computer Physics Reports 3, 71-124.

J.J. Monaghan, 1989. On the problem of penetration in particle methods. Journal of Computational Physics 82:1-15.

J.J. Monaghan, 1992. Smoothed Particle Hydrodynamics. Annual Review of Astronomy and Astrophysics 30, 543-574.

J.J. Monaghan, 1994. Simulating free surface flows with SPH. J. Comput. Phys. 110, 399-406.

J.J. Monaghan, Andrew Kos, 1999. Solitary waves on a Cretan beach. Journal of Waterway Port Coastal and Ocean Engineering-asce 125, 145–154.

Kasper, T., Steenfelt, J.S., Pedersen, L.M., Jackson, P.G., Heijmans, R.W.M.G., 2008. Stability of and submerged tunnel in offshore conditions under deep water wave impact. Coast Eng. 55 (9), 753–760.

Liu, M.B., Liu, G.R., 2010. Smoothed Particle Hydrodynamics (SPH): an Overview and Recent Developments. Arch Computat Methods Eng 17, 25–76.

M. Antuono, A. Colagrossi, S. Marrone, 2012. Numerical diffusive terms in weakly-compressible SPH schemes. Computer Physics Communications 183, 2570-2580.

M. Antuono, S. Marrone, A. Colagrossi, B. Bouscasse, 2015. Energy balance in the δ-SPH scheme, Computer Methods in Applied Mechanics and Engineering 289, 209-226.

Mashy David Green, 2016. Sloshing simulations with the smoothed particle hydrodynamics (SPH) method. PhD thesis, Imperial College London.

Morteza Bayareh, Amireh Nourbakhsh, Fardin Rouzbahani, Vahid Jouzaei. Explicit incompressible SPH algorithm for modelling channel and lid-driven flows. SN Applied Sciences 2019; 1: 1040.

Nagel, G.W., 2011. Dynamic Behavior of Tunnel Elements during the Immersion Process. M. Sc. Thesis. Delft University of Technology, p. pp142.

Peng, W., Lee, K.-H., Shin, S.-H., Mizutani, N., 2013. Numerical simulation of interactions between water waves and inclined-moored submerged floating breakwaters. Coast. Eng. 82, 76–87.

Peng, S., Wu, W.G., Chen, K.Q., et al. Experimental investigation on element immersing process of immersed tube tunnel of Hong Kong-Zhu Hai-Macao Bridge[C]. ASME 31st Int. Conf., 2012:1-7.

Ren, B., He, M., Dong, P., Wen, H., 2015. Nonlinear simulations of wave-induced motions of a freely floating body using WCSPH method. Appl. Ocean Res 50, 1–12.

Rémi A. Carmigniani, Damien Violeau, 2018. Optimal sponge layer for water waves numerical models. Ocean Engineering 163, 169-182.

Wendland, H, 1995. Piecewise polynomial, positive definite and compactly supported radial functions of minimal degree. Adv Comput Math 4, 389–396. https://doi.org/10.1007/BF02123482.